2018 26th Mediterranean Conference on Control and Automation (MED)
Zadar, Croatia, June 19-22, 2018

Development of a Tendon-Driven Robotic Tool targeting Visual-Servoing Minimally-Invasive Surgical Operations

Nikolaos Evangeliou[†], Petros Tsampiras[‡], and Anthony Tzes[†]

***Abstract*— The development and experimental evaluation of a prototype robotic surgical tool is presented in this article. Servo motors are used as actuators in a tendon-driven actuation mechanism. The 2 Degree-of-Freedom (DoF) manipulator is a cascade configuration of 2 rotational joint modules. Each DoF is actuated independently by the corresponding tendon pair in a pulley-driven configuration. The design, fabrication and kinematics of the tool are analyzed. Moreover, the efficiency of the overall system is investigated in experimental studies, utilizing two performance evaluation methods. The first is an IMU-based, whilst the second utilizes a monocular visual servoing setup.**

I. INTRODUCTION

In recent years research for robot-assisted Minimally Invasive Surgical (MIS) procedures has significantly increased and revolutionized the medical field by improving not only the surgeon's performance and accuracy, but most importantly the patient's recovery time [1], [2]. Additionally, advantages offered over traditional surgery include, but are not limited to, lower infection risk, teleoperation and superior optics. These advantages come at an increased cost, lack of haptic feedback and lack of intuitiveness, which researchers try to overcome [3].

In the rapidly growing MIS market, few commercialized systems have appeared for general surgery, such as the DaVinci [4] and the ALF-X [5] systems. Similar experimental platforms, featuring 2 Degrees-of-Freedom (DoF) at the robot's tip are the Raven [6], targeting mobility, the SOFIE robot [7], targeting force feedback at the tip, as well as the [8] targeting mobility in MIS operations.

Apart from the daVinci robot, the platforms presented feature antagonistic tendon-driven actuation, thus one DC-motor per tendon. In future MIS robotic systems for single incision surgery, such as those presented in [9]–[11], an increased number of DoF is utilized so as to enhance dexterity. The latter, however, would lead to high cost and increased volume systems, owing to the high number of motors for antagonistic actuation.

One way to solve this issue is to use different ways of actuation mechanisms such as those investigated in [12], [13]. Out of the presented methods, pneumatic actuation [14] should be omitted, due to the increase in size and control complexity it poses. Shape Memory Alloy (SMA) actuation, on the contrary, can aid miniaturization and cost reduction. Relevant work has appeared in [15]–[18]. However, the developed systems feature low bandwidth and payload capacity, thus it is generally considered that SMA actuation cannot be efficiently utilized for tissue manipulation tasks.

In this paper, a prototype MIS robotic probe is implemented. The resulting tool is tendon-driven and servo motors are used for the actuation of each DoF. Each antagonistic pair is assigned to a single servo-motor in a pulley drive configuration. A visual feedback system is employed to online track the tool's motion and the results are compared to an IMU-based tracking approach. The software is open-source and utilizes the Robot Operating System (ROS) as middleware. The novelty of the system relies within the utilization of a single servo-motor for actuation per DoF, the low weight and dimensions, the sufficient repeatability shown during experimentation and the visual-servoing readiness of the implementation.

In Section II the design and kinematic analysis of the fabricated surgical probe is presented. The control concept is presented and a vision-based pose estimation algorithm is extracted in Section III. The latter is evaluated and compared to an IMU-based positioning experiment, so as to evaluate the future potential of the implementation in Section IV.

II. DESIGN AND ANALYSIS OF A TENDON-DRIVEN MIS-ROBOTIC TOOL

A. Design of the Tendon-Driven Robotic Tool

1) Robotic Probe Structure: The surgical probe comprises of a series of three links in a cascade configuration as shown in Fig. 1. Two rotational joints are formed at the links' connection axis, with their axes of rotation perpendicular to each other. The links were designed and manufactured in-house using $T6065$ grade aluminum. The outer diameter of the tool is 10mm making it suitable for minimal access. The tool bears a 2.5mm middle working channel, allowing for utilization of surgical instrumentation such as biopsy needles, forceps or sensing modalities.

Two medical grade steel wires with a diameter of 0.5mm and a shear break force of 120N are used for each DoF's actuation. Channels of 0.8mm in diameter are formed to pass the wires through the links and attach them at a diameter of 2.5mm *w.r.t.* the middle working channel for actuation.

2) Actuator Selection: Dynamixel servo-motors were selected for actuation. They feature an accuracy of 0.088°, low weight and compact size and an embedded real-time controller with a single $RS485$ communication/power bus. The motors are placed at the back portion of the tool to

†Nikolaos Evangeliou and Anthony Tzes are with the Engineering Division, Electrical & Computer Engineering Program, New York University Abu Dhabi, Saadiyat Island, P.O.Box 129188, Abu Dhabi, United Arab Emirates

‡Petros Tsampiras is with the Electrical & Computer Engineering Department, University of Patras, 26500, Rio, Greece

Corresponding author's email: `anthony.tzes@nyu.edu`

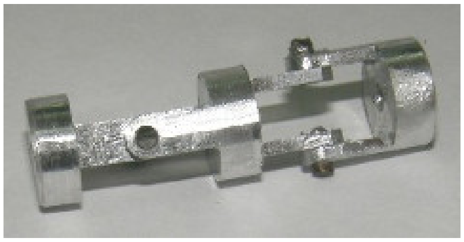

Fig. 1: Cascade links and joint formation

avoid contact with human tissue. The attachment of the tendons to the shaft of the motor forms a pulley configuration for antagonistic actuation. The overall mechanical setup is rendered in Fig. 2 and the physical implementation is depicted in Fig. 7b. The overall weight is 1kg.

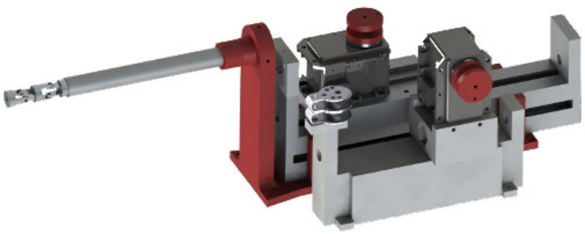

Fig. 2: Mechanical setup

B. Kinematic modelling of the surgical probe

1) Direct kinematics: The forward kinematics can be extracted using the Denavit-Hartenberg (DH) notation. The coordinate frame setting is given in Fig. 3, where the black dot represents the origin of the tool. The resulting DH parameters are summarized in Table I, where $l_1 =$ 17mm $l_2 = 10.5$mm and $\theta_i \in [-73.5^o, 73.5^o], i = 1,2$ owing to mechanical limitations.

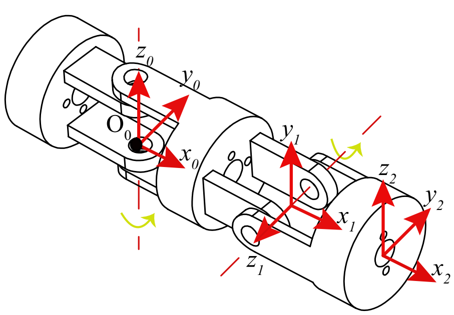

Fig. 3: Tool's coordinate frame assignment

TABLE I: Denavit-Hartenberg parameters

Joint	θ_i	a_i	α_i	d_i
1	θ_1	l_1	$\frac{\pi}{2}$	0
2	θ_2	l_2	$-\frac{\pi}{2}$	0

Thus, the homogenous transformation matrix from the probe's base to the tip is formulated in Eq. 1, where $c_i = \cos(\theta_i)$, $s_i = \sin(\theta_i)$. The resulting workspace is derived in Fig. 4.

$$T_0^2 = \begin{bmatrix} c_1c_2 & -s_1 & -c_1s_2 & l_2c_1c_2 + l_1c_1 \\ s_1c_2 & c_1 & -s_1s_2 & l_2s_1c_2 + l_1s_1 \\ s_2 & 0 & c_2 & l_2s_2 \\ 0 & 0 & 0 & 1 \end{bmatrix} \tag{1}$$

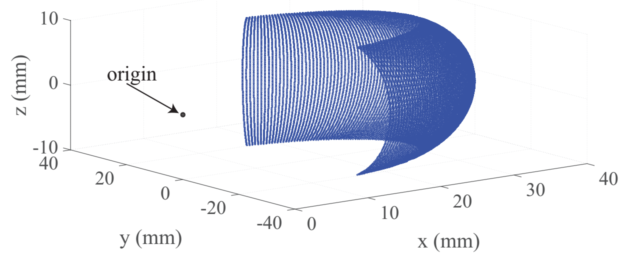

Fig. 4: Surgical tool workspace.

2) Inverse kinematics: Since only two kinematic parameters are unknown to the inverse kinematic problem, only two of the position or orientation variables are needed to reach a single solution to the problem. For example, given positions y_d and z_d in cartesian space, the solution is given by Eq. 2.

$$\theta_1 = \arcsin\left(\frac{y_d}{l_1 + l_2s_2}\right), \ \theta_2 = \arcsin\left(\frac{z_d}{l_2}\right) \tag{2}$$

3) Kinematic mappings: The kinematic model of the fabricated tool comprises of the four mappings shown in Fig. 5. These mappings represent the transformations between the various spaces of the kinematic model.

- User Space : It describes the end-effector position (x_d, y_d, z_d). The corresponding desired angles θ_1^d, θ_2^d of the joints can then be derived by the inverse kinematics solution presented in Eq. 2, to move towards actuator space.
- Actuator Space : We define the single joint's geometry, depicted in Fig. 6, where the black dot represents the axis of rotation. We assume a rotation of $\hat{\theta}^\circ$ and a tendon displacement of ΔL from its initial length $\tilde{L}_{init}$ for $\theta_1 = \theta_2 = 0^\circ$. The parameters ρ_i, L_i, d_i are a priori known by design, where in our case $\rho_1 =$ 1.95mm, $\rho_2 = 6.25$mm, $L_i = L_{i-1} = 8.5$mm and $d_i =$ $d_{i-1} = 2$mm. Then the unknown parameters of Fig. 6 can be geometrically computed from Eq. 3.

$$\begin{aligned} R &= \sqrt{\rho_1^2 + (L_{i-1} - d_i)^2} \ , \ R' = \sqrt{\rho_2^2 + (L_i - d_i)^2} \\ \hat{\kappa} &= \arctan\left(\frac{\rho_1}{L_{i-1} - d_i}\right) \ , \ \hat{\lambda} = \arctan\left(\frac{\rho_2}{L_i - d_i}\right) \\ \hat{\xi} &= \arccos\left(\frac{R^2 + R'^2 - \tilde{L}_i^2}{2RR'}\right). \end{aligned} \tag{3}$$

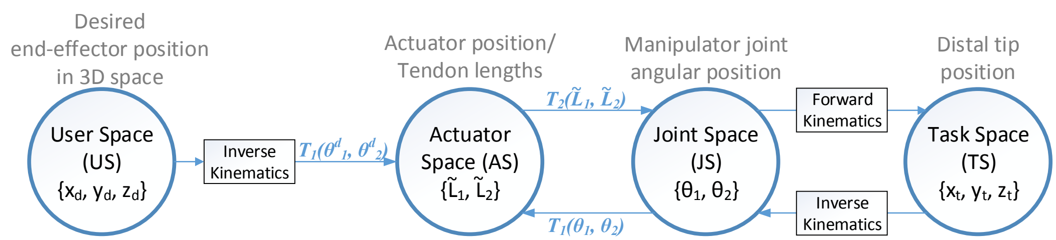

Fig. 5: Kinematic mappings

Given the known desired joint angles θ_1^d and θ_2^d, the tendon lengths can be computed as:

$$\begin{cases} \tilde{L}_1 = \sqrt{R^2 + (R')^2 + 2RR' \cos\left(\theta_1^d + \arctan\left(\frac{\rho_1}{L_{i-1} - d_i}\right) + \arctan\left(\frac{\rho_2}{L_i - d_i}\right)\right)} \\ \tilde{L}_2 = \sqrt{R^2 + (R')^2 + 2RR' \cos\left(\theta_2^d + \arctan\left(\frac{\rho_1}{L_{i-1} - d_i}\right) + \arctan\left(\frac{\rho_2}{L_i - d_i}\right)\right)} \end{cases}$$

The tendon lengths are then utilized in order to extract the required actuators' rotation rot_1 and rot_2.

$$rot_i = \frac{\tilde{L}_{init} - \tilde{L}_i}{r} \tag{4}$$

where $i = 1, 2$, $r = 2.4$mm the radius of tendon attachment to the servo-motor's shaft and $L_{init} = 13.69$mm the initial length of the tendon for $\theta_i = 0°, \mathrm{i} = 1, 2$.

- Joint Space: This space represents the tool's actual joint angles θ_1, θ_2 after the rotation of the actuators by rot_1 and rot_2. For known tendon lengths, the parameters θ_1, θ_2 are derived by:

$$\begin{cases} \theta_1 = \pi - \left[\arctan\left(\frac{\rho_1}{L_{i-1} - d_i}\right) + \arctan\left(\frac{\rho_2}{L_i - d_i}\right) + \arccos\left(\frac{R^2 + (R')^2 - \tilde{L}_1^2}{2RR'}\right)\right] \\ \theta_2 = \pi - \left[\arctan\left(\frac{\rho_1}{L_{i-1} - d_i}\right) + \arctan\left(\frac{\rho_2}{L_i - d_i}\right) + \arccos\left(\frac{R^2 + (R')^2 - \tilde{L}_2^2}{2RR'}\right)\right] \end{cases}$$

  where $\tilde{L}_1$ and $\tilde{L}_2$ the corresponding a priori known tendon lengths between two successive links, as in Fig. 6.
- Task Space: In this case the tool's distal tip position in Cartesian space is given by Eq. 1.

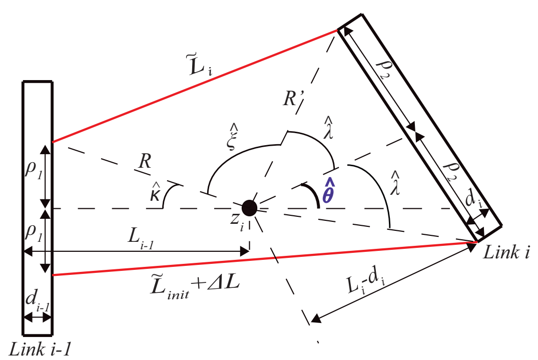

Fig. 6: Link and corresponding joint's geometry

III. Experimental Studies

Due to the medical nature of the application external sensory modalities cannot be utilized in a real surgical scenario. Thus, the online computation of the surgical probe's end-effector position can solely rely on feedback from the servo motors. Based on this, the repeatability of the tool is evaluated using a visual-servoing implementation based on passive marker detection and an IMU-based approach. The developed manipulator's motion software runs under ROS middleware at 100Hz.

A. Control Scheme

A simple yet effective controller is used to control each individual servo-motor's angular position. The control scheme comprizes of:

- The tendon length computation using the transition from joint space to actuator space described in Section II-B.3.
- A constant offest angular value equal to 8° and 18° for the first and second DoF respectively, aiming to compensate for tendon slackening during motion, as well as non-linear phenomena, such as cable-pulley friction [19].
- The embedded PID controller of the servo motor with adjustable PID gains for position control. In our case, the gains were selected experimentally to be equal to $\mathrm{K}_P = 20$, $\mathrm{K}_I = 5$, $\mathrm{K}_D = 0.1$.

B. Visual Servoing

The visual servoing system is based on the passive marker detection method of ArUco [20]. A 5x5cm rectangular marker was attached to the surgical probe's tip and a fixed imaging modality with a resolution of 1280x720pixel at 30fps was used for acquisition. The experimental setup is depicted in Fig. 7a and the detection loop runs at 20Hz.

The probe's response to various reference joint angles are computed using the optical tracking utility and converted using forward kinematics to corresponding coordinates of the tool's tip in 3D space, as shown in Fig. 8.

The figures depict a positioning accuracy of no more than 0.5mm per axis, or 0.59mm in 3-D space. A lag time of approximately 1 sec is observed at the beginning of each motion, due to tendon slackening on the pulleys. The spikes occurring during the transitional state of the tool's motion are mainly attributed to the noise of the optical measurement system.

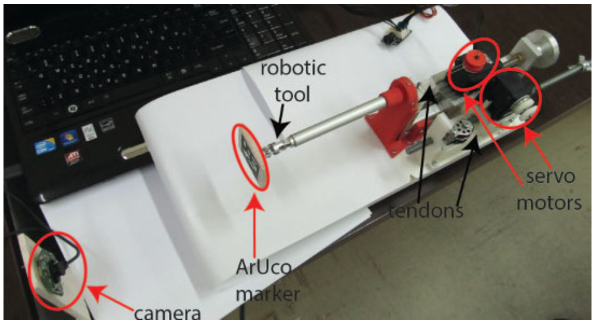

(a) ArUco experimental setup

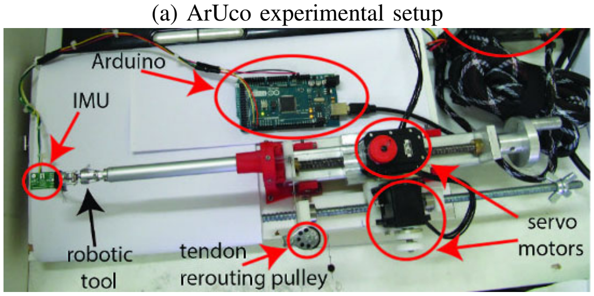

(b) IMU evaluation setup

Fig. 7: Experimental setups

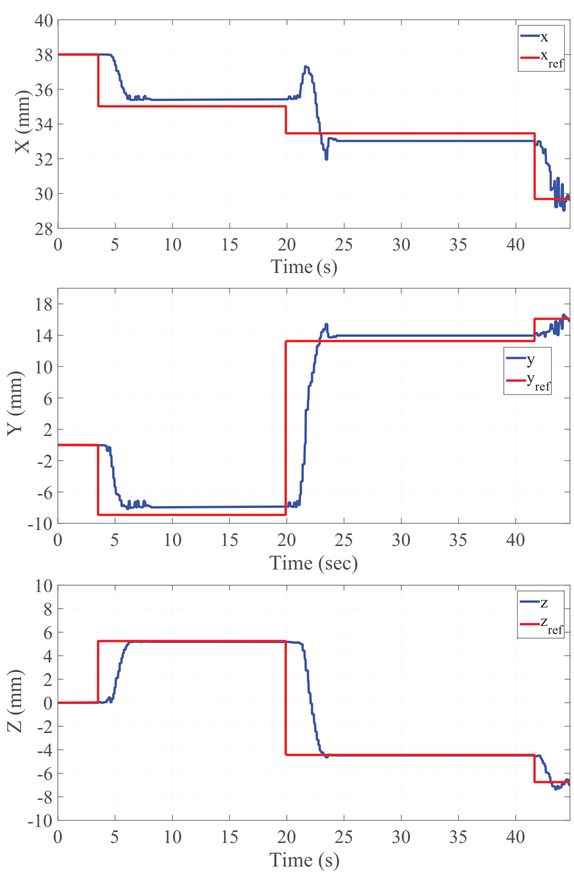

Fig. 8: ArUco evaluation - End effector position

C. Evaluation with IMU-based measurement system

Supplementary to the optical tracking algorithm, a 9-DoF IMU sensor was attached at the distal end of the tool, shown in Fig 7b, in order to estimate the robot's pose. The measurements of the gyroscope, accelerometer and magnetometer were fused using the Direct Cosine Matrix method described in [21].

For random reference motion commands, the resulting coordinates of the tool's distal tip are shown in Fig. 9. The maximum error observed during motion is 0.95mm. Similarly, the rapid motion from $\theta_1 = \theta_2 = 0°$ to the workspace's extremities is depicted in Fig. 10.

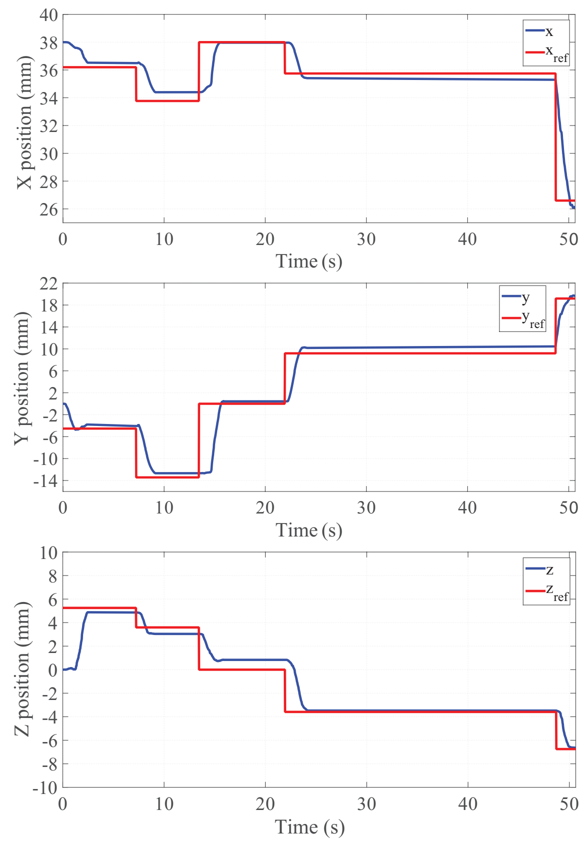

Fig. 9: IMU masured tip's position per axis

In order to determine the payload capacity of the fabricated tool, varying weight was placed at its end of the tool and measurements were taken with the IMU setup. The resulting responses for the second DoF are shown in Fig. 11. A maximum payload of 4N is observed. Similar values were observed for the first DoF.

IV. CONCLUSIONS

A prototype robotic tool with tendon-driven configuration and servo actuation for minimally-invasive surgical operations was fabricated and evaluated. The accuracy of the tool's motion was experimentally tested by varying methods and the resulting accuracy makes it suitable for future clinical exploitation.

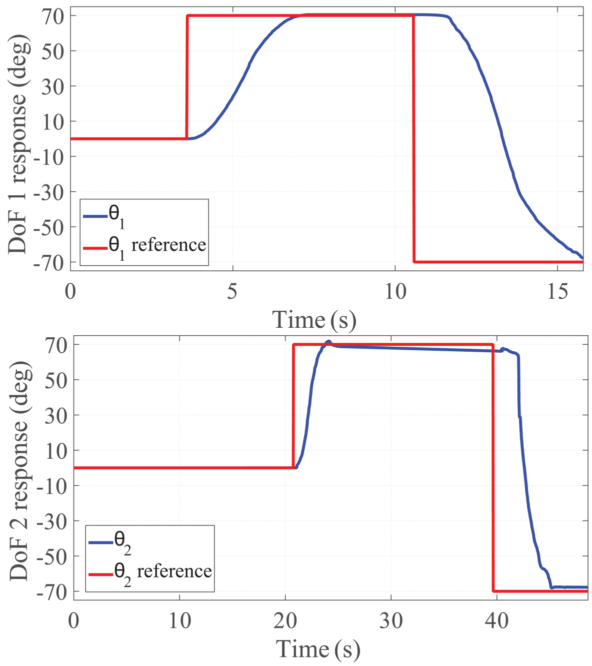

Fig. 10: IMU based DoFs' step responses at extremities

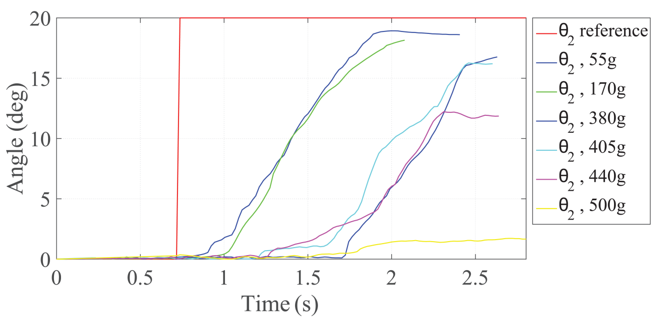

Fig. 11: DoF 2 step response under varying payload

REFERENCES

[1] V. Vitiello, S. L. Lee, T. P. Cundy, and G. Z. Yang, "Emerging robotic platforms for minimally invasive surgery," *IEEE Reviews in Biomedical Engineering*, vol. 6, pp. 111–126, 2013.

[2] E. A. Arkenbout, P. W. Henselmans, F. Jelinek, and B. Paul, "A state of the art review and categorization of multi-branched instruments for notes and sils," *Surgical Endoscopy*, vol. 29, no. 6, pp. 1281–1296, 2015.

[3] C. Tsui, R. Klein, and M. Garabrant, "Minimally invasive surgery: national trends in adoption and future directions for hospital strategy," *Surgical Endoscopy*, vol. 27, no. 7, pp. 2253–2257, 2013.

[4] G. S. Guthart and J. K. Salisbury, "The IntuitiveTM telesurgery system: overview and application," in *Proceedings 2000 ICRA. Millennium Conference. IEEE International Conference on Robotics and Automation. Symposia Proceedings (Cat. No.00CH37065)*, vol. 1, San Francisco, CA, USA, 2000, pp. 618–621.

[5] V. Larocca, F. Marino, A. Filippis, S. Gidaro, and A. Lococo, "A new operative telesurgical system: Telelap alf-x - experimental study on animal model," vol. 2, pp. 12–15, 01 2014.

[6] M. J. H. Lum, D. C. W. Friedman, G. Sankaranarayanan, H. King, K. Fodero, R. Leuschke, B. Hannaford, J. Rosen, and M. N. Sinanan, "The raven: Design and validation of a telesurgery system," *The International Journal of Robotics Research*, vol. 28, no. 9, pp. 1183–1197, 2009.

[7] L. van den Bedem, R. Hendrix, N. Rosielle, M. Steinbuch, and H. Nijmeijer, "Design of a minimally invasive surgical teleoperated master-slave system with haptic feedback," in *2009 International Conference on Mechatronics and Automation*, Aug 2009, pp. 60–65.

[8] J. Troccaz, U. Hagn, M. Nickl, S. Jörg, G. Passig, T. Bahls, A. Nothhelfer, F. Hacker, L. Le-Tien, A. Albu-Schäffer, *et al.*, "The DLR MIRO: a versatile lightweight robot for surgical applications," *Industrial Robot: An International Journal*, vol. 35, no. 4, pp. 324–336, 2008.

[9] J. Rosen, L. N. Sekhar, D. Glozman, M. Miyasaka, J. Dosher, B. Dellon, K. S. Moe, A. Kim, L. J. Kim, T. Lendvay, Y. Li, and B. Hannaford, "Roboscope: A flexible and bendable surgical robot for single portal minimally invasive surgery," in *2017 IEEE International Conference on Robotics and Automation (ICRA)*, May 2017, pp. 2364–2370.

[10] A. Degani, H. Choset, A. Wolf, and M. A. Zenati, "Highly articulated robotic probe for minimally invasive surgery," in *Proceedings 2006 IEEE International Conference on Robotics and Automation, 2006. ICRA 2006.*, May 2006, pp. 4167–4172.

[11] K. S. Roh, S. Yoon, Y. Do Kwon, Y. Shim, and Y.-J. Kim, "Single-port surgical robot system with flexible surgical instruments," in *Intelligent Robotics and Applications*, H. Liu, N. Kubota, X. Zhu, R. Dillmann, and D. Zhou, Eds. Springer International Publishing, 2015, pp. 447–459.

[12] H. M. Le, T. N. Do, and S. J. Phee, "A survey on actuators-driven surgical robots," *Sensors and Actuators A: Physical*, vol. 247, pp. 323 – 354, 2016.

[13] E. Kolyvas, Y. Koveos, and A. Tzes, "Sliding mode-based control of thin shape memory alloy actuators using a spatial hysteresis approximation," *Mechatronics*, vol. 40, pp. 115–127, 2016.

[14] K. Tadano and K. Kawashima, "Development of a master slave system with force sensing using pneumatic servo system for laparoscopic surgery," in *Proceedings 2007 IEEE International Conference on Robotics and Automation*, April 2007, pp. 947–952.

[15] E. Tzorakoleftherakis, A. Mavrommati, and A. Tzes, "Design and implementation of a binary redundant manipulator with cascaded modules," in *Journal of Mechanisms and Robotics*, vol. 8, no. 1, 2016, p. 011002.

[16] N. Evangeliou and A. Tzes, "Development of an sma-actuated redundant robotic platform for minimally invasive surgery," in *2016 6th IEEE International Conference on Biomedical Robotics and Biomechatronics (BioRob)*, June 2016, pp. 353–358.

[17] M. Ho, A. B. McMillan, J. M. Simard, R. Gullapalli, and J. P. Desai, "Toward a meso-scale sma-actuated mri-compatible neurosurgical robot," *IEEE Transactions on Robotics*, vol. 28, no. 1, pp. 213–222, Feb 2012.

[18] N. Evangeliou and A. Tzes, "Design and control of a robotic platform for dexterous minimally invasive surgical applications," *International Review on Automatic Control (IREACO)*, vol. 10, no. 5, pp. 443–450, 2017.

[19] M. Miyasaka, J. Matheson, A. Lewis, and B. Hannaford, "Measurement of the cable-pulley coulomb and viscous friction for a cable-driven surgical robotic system," in *2015 IEEE/RSJ International Conference on Intelligent Robots and Systems (IROS)*, Sept 2015, pp. 804–810.

[20] S. Garrido-Jurado, R. M. noz Salinas, F. Madrid-Cuevas, and M. Marín-Jiménez, "Automatic generation and detection of highly reliable fiducial markers under occlusion," *Pattern Recognition*, vol. 47, no. 6, pp. 2280 – 2292, 2014.

[21] W. Premerlani and P. Bizard, "Direction cosine matrix imu: Theory," *Diy Drone: Usa*, pp. 13–15, 2009.